IEEE Access
Multidisciplinary ⋮ Rapid Review ⋮ Open Access Journal

Received March 28, 2021, accepted April 13, 2021, date of publication April 29, 2021, date of current version May 10, 2021.

Digital Object Identifier 10.1109/ACCESS.2021.3076578

Towards Autonomous Aerial Scouting Using Multi-Rotors in Subterranean Tunnel Navigation

CHRISTOFOROS KANELLAKIS[1], PETROS S. KARVELIS[1], SINA SHARIF MANSOURI[1], (Member, IEEE), ALI-AKBAR AGHA-MOHAMMADI[2], AND GEORGE NIKOLAKOPOULOS[1]

[1]Department of Computer Science, Space and Electrical Engineering, Robotics Team, Luleå University of Technology, 97187 Luleå, Sweden
[2]Jet Propulsion Laboratory, California Institute of Technology, Pasadena, CA 91109, USA

Corresponding author: Christoforos Kanellakis (chrkan@ltu.se)

This work was supported in part by the Interreg Nord Programme ROBOSOL NYPS 20202891, and in part by the European Union's Horizon 2020 Research and Innovation Programme through illuMINEation under Grant 869379.

ABSTRACT This work establishes a robocentric framework around a non-linear Model Predictive Control (NMPC) for autonomous navigation of quadrotors in tunnel-like environments. The proposed framework enables obstacle free navigation capabilities for resource constraint platforms in areas with critical challenges including darkness, textureless surfaces as well as areas with self-similar geometries, without any prior knowledge. The core contribution of the proposed framework stems from the merging of perception dynamics in a model-based optimization approach, aligning the vehicles heading to the tunnels' open space expressed in the x axis coordinate in the image frame of the most distant area. Moreover, the aerial vehicle is considered as a free-flying object that plans its actions using egocentric onboard sensors. The proposed method can be deployed in both fully illuminated indoor corridors or featureless dark tunnels, leveraging visual processing from either RGB-D or monocular sensors for generating direction commands to keep flying in the proper direction. Multiple experimental field trials demonstrate the effectiveness of the proposed method in challenging environments.

INDEX TERMS Perception aware control, vision based navigation, micro aerial vehicles.

I. INTRODUCTION

The quest for autonomous MAVs that can reliably navigate in partially-known or unknown areas brings these platforms in the forefront of research and technological breakthroughs, while introducing novel approaches for several application areas. Infrastructure inspection [1], search and rescue [2], area coverage/surveillance [3] are fields that already pursue the incorporation of aerial vehicles in their operation cycles. These applications can be part of large scale outdoors environments (e.g. bridges, wind-turbines, power plants), urban environments (e.g. cities) and subterranean operating environments (e.g. tunnels and cave networks).

This article approaches the problem of autonomous navigation of low-cost aerial robots, referred with the term ''aerial scouts'', which is a subcomponent of the NeBula autonomy framework [4], related to multi-robot exploration missions in complex environments [5]–[7]. Aerial scouts can be defined as consumable vehicles with the main mission to explore high risk areas, collect sensor data (e.g. laser measurements, thermal, visual, gas, etc) for the operators to safely assess the status of the infrastructure. The baseline capability of these platforms is to navigate along a tunnel-like environments while returning close to their takeoff position. The proposed architecture couples a Nonlinear Model Predictive Control (NMPC) with a visual processing scheme in the local frame of the robot for maintaining proper obstacle free direction along the tunnel axis, following the open space area described with the furthest distance in depth images.

A. BACKGROUND & RELATED WORKS

Several works in the existing literature have addressed the control and navigation of MAVs in challenging environments using various sensor configurations. In [8] the fields of estimation, control and mapping for the MAV's autonomous navigation along penstocks, have been studied. In this work the major sensors used were a laser range finder and 4 cameras for the task of state estimation and mapping. In [9] a range

The associate editor coordinating the review of this manuscript and approving it for publication was Shun-Feng Su.

based sensor array approach has been developed to navigate along right-rectangular tunnels and cylindrical shafts. The authors proposed a range sensor configuration, to improve the localization in such environments and provide the means for autonomous navigation. In [10], the authors presented a multi-modal sensor unit for mapping applications, a means for aerial robots to navigate in dark underground tunnels. In this work, the unit consists of a stereo camera, a depth sensor, an IMU and led lights syncs with the camera capture for artificial lightning. Furthermore, the unit has been integrated with a volumetric exploration method, demonstrating the capabilities of the overall system. Regarding vision based optimal predictive control not many works have addressed the coupling of the control actions with vision, that can act as the planner for autonomous navigation. In [11] a perception-aware Model Predictive Control (MPC) algorithm has been proposed to compute trajectories for quadrotors that maximize the visibility of a desired target, optimizing both the action and perception objectives. This method leverages numerical optimization to compute feasible trajectories solving an optimization problem, where the cost function respects both the robot dynamics and perception objectives. In [12] a collision avoidance scheme has been presented that guides an aerial vehicle around an object along a conical spiral trajectory using a spherical camera model in a visual predictive control. In this work the vehicle dynamics have been linearized and partitioned in two parts, the first part includes the z axis and the second part the x and y axes, leading to two individual controllers that provide the control actions for the low level control. The image and z axis of the vehicle's dynamics are included in a process model and the nonlinear optimization problem is solved over the derived common state. Other works on vision based control have approached the navigation from other aspects, such in [13] where the authors proposed a method to guide a multirotor to a desired pose, while simultaneously keeping a target within the field of view of the onboard camera. In this work visual servoing scheme is used to generate a trajectory based on the minimization of the target re-projection error, while an MPC scheme was developed to track the trajectory. In [14] the authors presented a hybrid visual servoing scheme for deferentially flat systems formulated as an optimal control. The method initially computed the final pose of the vehicle using the desired camera view by solving a Perspective-n-Point problem and then used optimal control to compute a feasible trajectory, with a cost function to keep the image features in the view. In [15] the authors presented a cascaded formulation of IBVS and Linear MPC control scheme, with the aim to tackle the under-actuation issues related to the integration of IBVS on quadrotors. In this work the authors provide feasibility and stability guarantees of the MPC. Compared to the State-of-the-art, this work proposes an alternative architecture on the high level model based control for MAVs, which integrates visual perception state in the command generation, to enable reactive fast exploration of unknown subterranean/urban tunnel environments. The presented

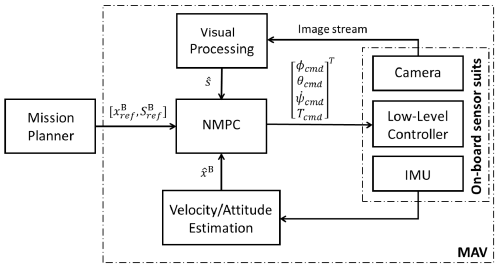

FIGURE 1. Overall block diagram of the proposed system, where signals X, S represent the vehicle and perception states, while signals θ_{cmd}, ϕ_{cmd}, $\dot{\psi}_{cmd}$ and T_{cmd} represent roll, pitch, yaw-rate and thrust commands for the low level controller.

control design is independent of x, y position or global map information, since localization can be an issue in complex, real-life underground areas. Table 1 summarizes the modules from all frameworks, depicting the alternative approaches on vision augmented optimal control for aerial platforms.

B. CONTRIBUTIONS

Based on the aforementioned state of the art, the major contribution of this article stems from the establishment of an aerial scout robot, capable to navigate along tunnels, leveraging visual data for keeping the proper direction along the tunnel, following open spaces identified through depth image processing. Initially, in the proposed architecture the platform is treated as a free-flying object following velocity, rather than precise position references on x and y axes, under the policy that velocity estimation can recover faster than position drift in degenerated environments, since reliable localization is still a major issue. Moreover, the control design incorporates a perception state in the MAV dynamics which is coupled with the yawrate control input. Thus allowing for a vision-driven direction control of the platform, since ''where to look'' is another major issue. Additionally, the fundamental component of the visual processing is the extraction of the free space in the tunnel, which is expressed through a 2D centroid in either a monocular image or an RGB-D depth image. The proposed control scheme can be directly deployed on a quadrotor with a camera and without requiring precise or even rough models of the surrounding areas or large training datasets. Finally, multiple field tests have been performed in different areas depicting the performance of the proposed method. More specifically, this work showcases field tests from a limited access to the public underground mine, providing valuable insights on the continuation of the research field.

C. OUTLINE

The rest of the article is structured as it follows. Section II describes the overall framework. Section III provides an overview of extended field trials on different scenarios and finally, Section IV presents the concluding remarks of the developed system.

II. AERIAL SCOUT FRAMEWORK

Figure 1 presents the overall proposed system architecture..

TABLE 1. MAV visual predictive control comparison.

Works	Control	Vision-Module	Navigation	Experimental Evaluation
[11]	Reference trajectory tracking MPC with 3D landmark visibility in image plane (perception states)	Feature extraction	Trajectory following with 3D landmark visibility, keeping it in the middle of the image plane and minimizing its velocity	Lab
[12]	Image based MPC design on spherical coordinates (perception states), incorporating conical spiral motion model	Object detection	Conical spiral trajectory generation for avoidance based on single point feature detection	Lab
[13]	Reference optimal trajectory generation with penalization on 3D landmark re-projection error and tracking NMPC	Fiducial marker processing for image frame coordinates and relative pose coordinates in camera frame	Trajectory generation to reach the goal pose of the 3D landmark, keeping the landmark in the middle of the image plane	Indoors
[14]	Reference dynamically feasible trajectory generation and tracking MPC, while maintaining substantial 2D image features	Requires initial and goal image. Feature tracking and PnP processing	Trajectory tracking to reach goal pose based on the provided goal image	Outdoors
[15]	Cascade IBVS and MPC velocity tracking	Feature extraction	Reach goal feature positions in image plane	Lab
Ours	Reference velocity, altitude and heading rate (perception state) tracking NMPC	Visual processing of monocular depth or RGB-D depth frames to identify centroid area of open space	Floating object velocity carrot chasing and reactive motion along tunnel axis yaw rate tracking	Underground mine tunnel & urban tunnel

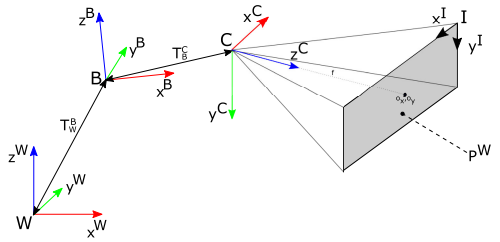

FIGURE 2. Coordinate frames, where $\mathcal{W}$, $\mathcal{B}$, $\mathcal{C}$ and $\mathcal{I}$ denote world, body and camera and image coordinate frames respectively.

A. PRELIMINARIES

The world frame $\mathcal{W}$ is fixed with the unit vectors $\{x^{\mathcal{W}}, y^{\mathcal{W}}, z^{\mathcal{W}}\}$ following the North-West-Up (NWU) frame convention. The body frame of the aerial vehicle $\mathcal{B}$ is attached on its base with the unit vectors $\{x^{\mathcal{B}}, y^{\mathcal{B}}, z^{\mathcal{B}}\}$. The $z^{\mathcal{B}}$ is antiparallel to the gravity vector, $x^{\mathcal{B}}$ is looking forward the platform's base and $y^{\mathcal{B}}$ is in the NWU convention. The onboard camera frame $\mathcal{C}$ has unit vectors $\{x^{\mathcal{C}}, y^{\mathcal{C}}, z^{\mathcal{C}}\}$. Furthermore, $y^{\mathcal{C}}$ is parallel to the gravity vector and $z^{\mathcal{C}}$ points in front of the camera. Finally, the image plane is defined as $\mathcal{I}$ with unit vectors $[x^{\mathcal{I}}, y^{\mathcal{I}}]$. Figure 2 depicts the utilized main coordinate frames of the aerial platform.

B. MAV DYNAMICS

The quadrotor model derived in [16] is used, providing roll ϕ_{cmd}, pitch $\theta_{cmd} \in [-\pi/2, \pi/2]$ and thrust $T_{cmd} \in \mathbb{R}_+$ commands, that are later handled by a low-level controller mounted onboard the aerial vehicle. Equation (1a) summarizes the quadrotor model.

$$\dot{p_z} = v_z^{\mathcal{B}} \tag{1a}$$

$$\begin{bmatrix} \dot{v}_x^{\mathcal{B}} \\ \dot{v}_y^{\mathcal{B}} \\ \dot{v}_z^{\mathcal{B}} \end{bmatrix} = R(\theta, \phi) \begin{bmatrix} 0 \\ 0 \\ T_d \end{bmatrix} + \begin{bmatrix} 0 \\ 0 \\ -g \end{bmatrix} - \begin{bmatrix} A_x & 0 & 0 \\ 0 & A_y & 0 \\ 0 & 0 & A_z \end{bmatrix} \begin{bmatrix} v_x^{\mathcal{B}} \\ v_y^{\mathcal{B}} \\ v_z^{\mathcal{B}} \end{bmatrix} \tag{1b}$$

$$\dot{\phi} = \frac{1}{\tau_\phi}(K_\phi \phi_{cmd} - \phi) \tag{1c}$$

$$\dot{\theta} = \frac{1}{\tau_\theta}(K_\theta \theta_{cmd} - \theta) \tag{1d}$$

where $\dot{p_z}$ is the relative distance of the platform with the ground $v^{\mathcal{B}} = [v_x^{\mathcal{B}}, v_y^{\mathcal{B}}, v_z^{\mathcal{B}}]^\top \in \mathbb{R}^3$ represents the linear velocities on each axis, $\phi, \theta \in \mathbb{R}$ are roll and pitch, $R \in SO(3)$ is the rotation matrix without a rotation around the z-axis, since the coordinates are in the body frame, $T_d \in \mathbb{R}$ is the mass normalized thrust, g is the gravitational acceleration, A_x, A_y, and A_z are the normalized mass drag coefficients, τ_ϕ and τ_θ are the time constants, and K_ϕ, K_θ are the roll and pitch angle gains, and finally ϕ_{cmd}, θ_{cmd} are the reference values of the roll and pitch angle for the low level controller. From [17], the model incorporates the mass normalized thrust T_d that is converted to T_{cmd} using the derived adaptive acceleration control scheme.

C. PERCEPTION STATE

Following the Image-based Visual Servoing (IBVS) theory [18] Equation (2) describes the desired relation in the 2D target motion represented by s_x and s_y coordinates and the 3D camera motion, with the assumption that the target is static.

$$\begin{bmatrix} \dot{s}_x \\ \dot{s}_y \end{bmatrix} = L \begin{bmatrix} v_x^{\mathcal{C}} & v_y^{\mathcal{C}} & v_z^{\mathcal{C}} & \omega_x^{\mathcal{C}} & \omega_y^{\mathcal{C}} & \omega_z^{\mathcal{C}} \end{bmatrix}^\top \tag{2}$$

where $v^{\mathcal{C}} = [v_x^{\mathcal{C}}, v_y^{\mathcal{C}}, v_z^{\mathcal{C}}]^\top \in \mathbb{R}^3$ and $\omega^{\mathcal{C}} = [\omega_x^{\mathcal{C}}, \omega_y^{\mathcal{C}}, \omega_z^{\mathcal{C}}]^\top \in \mathbb{R}^3$ represent the linear and angular velocities in frame $\mathcal{C}$, while the $L \in \mathbb{R}^{2\times 6}$ matrix that describes the coupling is called Interaction matrix and is defined as:

$$L = \begin{bmatrix} -\frac{1}{d(x^{\mathcal{I}}, y^{\mathcal{I}})} & 0 & \frac{s_x}{d(x^{\mathcal{I}}, y^{\mathcal{I}})} & s_x s_y & -1-s_x^2 & s_y \\ 0 & -\frac{1}{d(x^{\mathcal{I}}, y^{\mathcal{I}})} & \frac{s_y}{d(x^{\mathcal{I}}, y^{\mathcal{I}})} & 1+s_y^2 & -s_x s_y & -s_x \end{bmatrix} \tag{3}$$

where $d(x^{\mathcal{I}}, y^{\mathcal{I}}) = Z_P^{\mathcal{C}}$ and $d(\cdot)$ represents the depth map of the image $I(x^{\mathcal{I}}, y^{\mathcal{I}}), \forall x^{\mathcal{I}} \in columns$ and $y^{\mathcal{I}} \in rows$. The

interaction matrix L includes the depth $Z_P^{\mathscr{C}}$, information that is lost when working in the 2D image plane.

The rate of change of s_x is mainly affected when the camera is undergoing a yaw motion $\omega_y^{\mathscr{C}}$ and a lateral velocity v_x. The other camera motions have negligible effect in the rate of change of the target position in the image plane. In the case where s_x is closer to the center of the image, $\omega_y^{\mathscr{C}}$ has a greater impact in the rate of change when compared to the lateral velocity $v_x^{\mathscr{C}}$ of the camera and therefore $v_x^{\mathscr{C}}$ can be ignored. Equation (4) express the simplified image dynamics that consist the perception state.

$$\dot{s}_x = (1 + s_x^2)(\dot{\psi}_{cmd}) \tag{4}$$

D. VISUAL PROCESSING

The core concept in the proposed method is the identification of open space along the tunnel axis using the onboard visual sensor. The goal is to align the MAV heading towards open spaces, thus allowing the aerial platform to follow obstacle free paths. Extending the previous work [19], this article expands the concept of open space identification by processing depth images in two ways, firstly showcasing the general applicability of the method using depth map from RGB-D sensor for well illuminated areas and pseudo depth map monocular sensor in dark environments, while secondly connects the visual processing with the control framework by closing the loop.

1) SINGE IMAGE PSEUDO DEPTH ESTIMATION

This method describes the established methodology for calculating a pseudo depth map from single images, with the main aim to identify areas in the frame that are free space, without considering metric information. Using the light scattering [20] method an image can be defined as follows:

$$I(x^{\mathscr{I}}, y^{\mathscr{I}}) = O(x^{\mathscr{I}}, y^{\mathscr{I}}) \cdot tr(x^{\mathscr{I}}, y^{\mathscr{I}}) + a[1 - tr(x^{\mathscr{I}}, y^{\mathscr{I}})] \tag{5}$$

where $I : [0 \dots M-1] \times [0 \dots N-1] \rightarrow \mathbb{N}^2$ is the observed image, $O : [0 \dots M-1] \times [0 \dots N-1] \rightarrow \mathbb{N}^2$ is the original image, a is the color of the atmospheric light, $tr(x^{\mathscr{I}}, y^{\mathscr{I}})$ is the transmission term. The term $O(x^{\mathscr{I}}, y^{\mathscr{I}}) \cdot tr(x^{\mathscr{I}}, y^{\mathscr{I}})$ is called direct attenuation [21], while term $a[1 - tr(x, y)]$ is called airlight. The transmission term describes the amount of light that reaches the camera and is defined as:

$$tr(x^{\mathscr{I}}, y^{\mathscr{I}}) = e^{-\beta d(x^{\mathscr{I}}, y^{\mathscr{I}})} \tag{6}$$

where β is the scattering coefficient of the atmosphere and $d(x^{\mathscr{I}}, y^{\mathscr{I}})$ is the depth of the scene for the pixel coordinates $(x^{\mathscr{I}}, y^{\mathscr{I}})$. The Dark Channel Prior (DCP) [22] method is used to calculate the transmission map defined as follows:

$$tr(x^{\mathscr{I}}, y^{\mathscr{I}}) = 1 - \omega\Big[\frac{I^{dark}(x^{\mathscr{I}}, y^{\mathscr{I}})}{a}\Big] \tag{7}$$

$$I^{dark}(x^{\mathscr{I}}, y^{\mathscr{I}}) = \min_{C \in R,G,B} [\min_{z \in \Omega(x^{\mathscr{I}}, y^{\mathscr{I}})} I^C(z)] \tag{8}$$

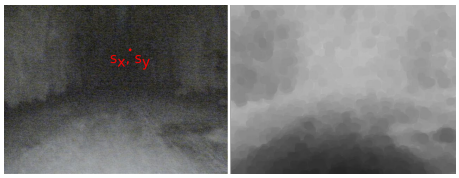

FIGURE 3. On the left onboard RGB image frame with the extracted centroid denoted with the red circle, while on the right the estimated pseudo depth image from a single image.

FIGURE 4. On the left onboard depth image frame from Intel RealSense ZR300, while on the right the processed depth image with the extracted centroid denoted with the red circle.

where ω is a number controlling the desired level of restoration with maximum value of 1, $I^{dark}(x^{\mathscr{I}}, y^{\mathscr{I}})$ is the dark channel, $\Omega(x^{\mathscr{I}}, y^{\mathscr{I}})$ is a patch of 5×5 pixels centered on $(x^{\mathscr{I}}, y^{\mathscr{I}})$, I^C is the color channel of the image I, z represents the index of the pixel of $\Omega(x^{\mathscr{I}}, y^{\mathscr{I}})$.

The atmospheric light is shown in Equation 9.

$$a = max \sum_{C=1}^{3} I^C \left\{ \underset{(x^{\mathscr{I}}, y^{\mathscr{I}}) \in (0.1\%h \times w)}{\arg\max} \left[I^{dark}\left(x^{\mathscr{I}}, y^{\mathscr{I}}\right) \right] \right\} \tag{9}$$

where w, h represent the width and height of I^{dark}.

This visual processing methodology, part of the proposed control framework, is employed to tackle the challenge of identifying the open space in tunnels and caves to regulate the aerial platform heading accordingly and operates in pitch dark tunnels without external illumination infrastructure.

In order to extract the centroid location of the area with the open space in the tunnel, represented as the area with the maximum distance from the MAV, we first employ a grey scale morphological operation in the depth map image [23] and in the sequel employ the *k-means* [24] algorithm in order to segment the depth image into a number of clusters defined as C_i, $i = 1, \dots, 10$. Finally, we compute the average intensity for each cluster and extract the s_x of the cluster with the maximum average intensity C_m from the depth map image [25]. The s_x of the cluster is the arithmetic mean of all x pixel coordinates in the cluster defined as:

$$s_x = \frac{1}{|C_m|} \sum_{(x,y) \in C_m} x \tag{10}$$

where $|C_m|$ is the number of pixels of the cluster. The overall method described in this section and impact on the centroid calculation are depicted in Figures 3, 4.

E. MISSION PLANNER

The system incorporates a higher level mission planner which is responsible to provide the references for the controller. The

mission planner initially accepts the desired state references from the operator once. Afterwards, a potential field obstacle avoidance method is activated, generating linear x-axis and y-axis reference velocity commands in order to avoid collisions to the walls or any other obstacle standing in the way of the MAV, as shown in [26].

F. CONTROL DESIGN

Compared to current State-of-the-Art the NMPC extends the non-linear dynamic model of the platform derived from (1a) by integrating the perception dynamics from (4). The state of the system is defined as $x^{\mathscr{B}}(t) = [\dot{p_z}, v_x^{\mathscr{B}}, v_y^{\mathscr{B}}, v_z^{\mathscr{B}}, \phi, \theta] \in \mathbb{R}^6$, where $\hat{x}^{\mathscr{B}}$ is the estimated state obtained from the onboard sensor measurements.

Moreover, the perception state vector $S(t) = s_x$ includes the visual states on the centroid, where $\hat{S}$ is the estimated state and the value $\hat{s}_x$ is provided from the visual processing unit discussed in Section II-D. The NMPC objective is to generate $u^{\mathscr{B}} = [\phi_{cmd}, \theta_{cmd}, \dot{\psi}_{cmd}, T_{cmd}]$ to keep the centroid in the center of the image and by doing this the MAV navigates along the tunnel, while following the tunnel altitude changes. Based on the obtained commands $u^{\mathscr{B}}$, the low-level controller generates motor commands for the MAV.

For the proposed NMPC, the finite horizon stage cost function is defined $l : \mathbb{R}^{n_x} \times \mathbb{R}^{n_S} \times \mathbb{R}^{n_u} \to \mathbb{R}_+$ and the terminal cost function $l_f : \mathbb{R}^{n_x} \times \mathbb{R}^{n_S} \to \mathbb{R}_+$, where n_x refers to the number of states, n_S refers to the number of the perception states and n_u refers to the number of commands.. The NMPC scheme can be formulated in the following equation for the problem of navigation in unknown tunnel-like environments:

$$
\begin{aligned}
\min_{\{u^{\mathscr{B}}_{k+j|k}\}_{j=0}^{N-1}} \; & lf_N\left(x^{\mathscr{B}}_{k+N|k}, S_{k+N|k}\right) \\
& + \sum_{j=0}^{N-1} l_{k+j|k}\left(x^{\mathscr{B}}_{k+j|k}, S_{k+j|k}, u^{\mathscr{B}}_{k+j|k}\right) \\
\text{s.t. } & x^{\mathscr{B}}_{k+j+1|k} = f(x^{\mathscr{B}}_{k+j|k}, u^{\mathscr{B}}_{k+j|k}),\ j \in \mathbb{N}_{[0,N-1]} \\
& S_{k+j+1|k} = g(v^{\mathscr{B}}_{z,k+j|k}, S_{k+j|k}, \dot{\psi}_{k+j|k}),\ j \in \mathbb{N}_{[0,N-1]} \\
& u^{\mathscr{B}}_{k+j|k} \in [u^{\mathscr{B}}_{\min}, u^{\mathscr{B}}_{\max}],\ j \in \mathbb{N}_{[0,N-1]} \\
& x^{\mathscr{B}}_{k|k} = \hat{x}^{\mathscr{B}}_{k} \\
& S_{k|k} = \hat{S}_k
\end{aligned} \tag{11}
$$

where $N \in \mathbb{N}$ is the control horizon, $u^{\mathscr{B}}_{\min}$ and $u^{\mathscr{B}}_{\max}$ are bounds on control actions. At every time instant k, a finite-horizon optimal problem is solved with a user defined interval, while a corresponding optimal sequence of control actions $u^{\star\mathscr{B}}_{k|k}, \ldots u^{\star\mathscr{B}}_{k+N-1|k}$ are generated, where the first control action $u^{\star\mathscr{B}}_{k|k}$ is applied to the low-level controller. In the next time instant the optimization solves the same problem by using the solution in the previous interval as the initial guess and updated information on current states value. More information of the structure and implementation of the PANOC controller can be found in [27].

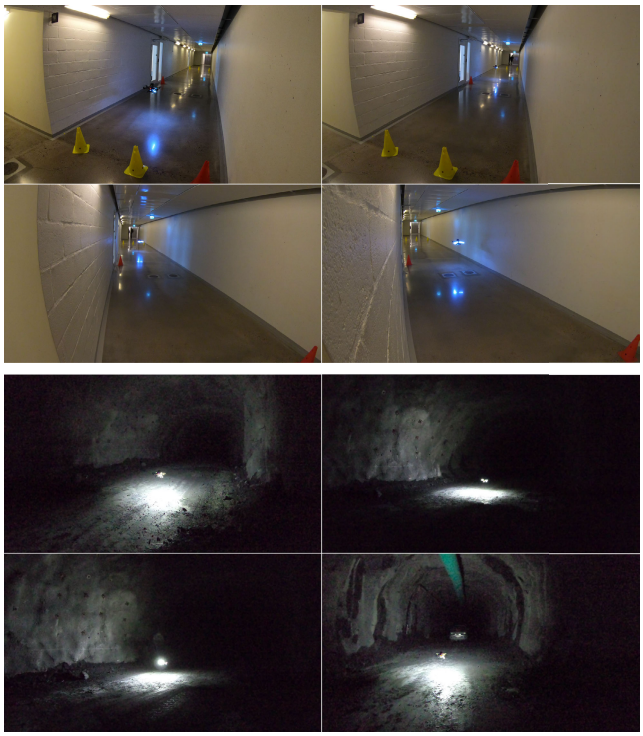

FIGURE 5. The top two rows depict snapshots from the experimental trials in the indoor corridor area, while the bottom rows depict the experimental trials in the underground tunnel.

III. EXPERIMENTAL RESULTS

In the performed field trials the aerial scout has been deployed in two different environments, a) an indoor corridor located at Luleå University of Technology and b) part of the production area of an iron ore mine in northern Sweden, located 1100 meters deep. The main concept of the system was to takeoff, move along the tunnel and return towards the takeoff position using a timer strategy, depicting navigation with return to base capabilities. The designed NMPC is mainly providing the yawrate command from the x axis open space in the image frame. Nevertheless, when the timer commands a turn the yawrate is fixed to a constant value and the centroid measurements are ignored until the rotation of approximately 180 deg is completed. The aim of these experiments is twofold a) to demonstrate the navigation capabilities of the platform without any prior knowledge of the area and b) to showcase that the method is applicable for totally different tunnel-like environments, while supporting different sensor modalities. It is of importance to note that the role of the resource constrained aerial scout is not to provide an accurate localization of any artifact or 3D map of the visited area, but rather navigate in extreme locations, collect raw sensor data and return in a location for the operator to retrieve it.

A. EXPERIMENTAL SETUP

In this work one aerial platform in two different configurations is used to evaluate the proposed method. The first configuration was used for the indoor corridor experiments and the second configuration for the underground tunnel

experiments. Generally, the vehicle weights 1.5 kg and provides 8 mins of flight time with 4-cell 1.5 Ah LiPo battery. The flight controller is ROSflight and the Aaeon UP-Board[1] is the main processing unit, incorporating an Intel Atom x5-Z8350 processor and 4 GB RAM. The operating system running on the board is Ubuntu Desktop 18.04 with ROS Melodic framework. In both scenarios the platform carried a 2D rotating Rplidar placed on top of the bodyframe, providing range measurements at 10Hz for the obstacle avoidance component, while the height measurements are provided from the single beam Lidar-lite v3 at 100 Hz installed on the bottom of the vehicle pointing down. Furthermore, the aerial platform is equipped with three 10 W LED light bars, two in both front arms and one facing downwards for providing additional illumination.

As mentioned above due to sensor limitations different sensors were employed for velocity estimation and the vision based open area identification. More specifically, in scenario a) the velocity estimation is based on IntelRealsense T265 at 200 Hz, installed on the backside of the vehicle pointing backwards, while for scenario b) the PX4Flow optical flow sensor at 20 Hz was installed on the bottom of the vehicle pointing down, since T265 had poor performance in darkness. Additionally, in scenario a) the depth camera RealSense ZR300 has been used to provide depth image at 20Hz, while in scenario b) the PS3 Eye camera has been used to generate pseudo depth images at 10 Hz and provide the x axis coordinate of the open space in the image plane. The onboard Inertial Measurement Unit (IMU) is used to provide the attitude states $[\phi, \theta]$ of the aerial platform, while the proposed framework does not require any position measurements on the x and y axis.

The NMPC has a prediction horizon of 40 steps, while the tuning parameters used by the NMPC were:

$$\begin{aligned} Q^x &= diag(5, 1, 1, 1, 3, 3), \quad Q_f^x = 10Q^x, \\ Q^S &= diag(10), \quad Q_f^S = 10Q^S, \\ R &= diag(2, 10, 10, 2) \end{aligned}$$

where *diag* denotes a square diagonal matrix. Additionally, in the control design, the following bounds have been considered as: $-0.4\,\text{rad/s} \leq [\phi_{cmd}, \theta_{cmd}, \dot{\psi}_{cmd}] \leq 0.4\,\text{rad/s}$ and $T_{cmd} \in [0, 1]$.

1) FIRST SCENARIO

In this case the environment is well-illuminated and the main challenge is that it's geometry is self-similar. the tunnel is 3 m wide and 3 m height, while the MAV navigated for 40 m forward and back. In this scenario the operator defined reference state vectors were $x_{ref} = [0.3\,\text{m/s}, 0, 0, 0, 0]$ and $S_{ref} = [0]$.

Furthermore, the first subfigure of Figure 6 presents the tracking of $v_x^{\mathcal{B}}$ to the desired reference. In this case the controller was able to follow the reference with Mean Absolute Error of 0.1 m/s. The velocity is tracking the desired values

[1]https://www.aaeon.com/

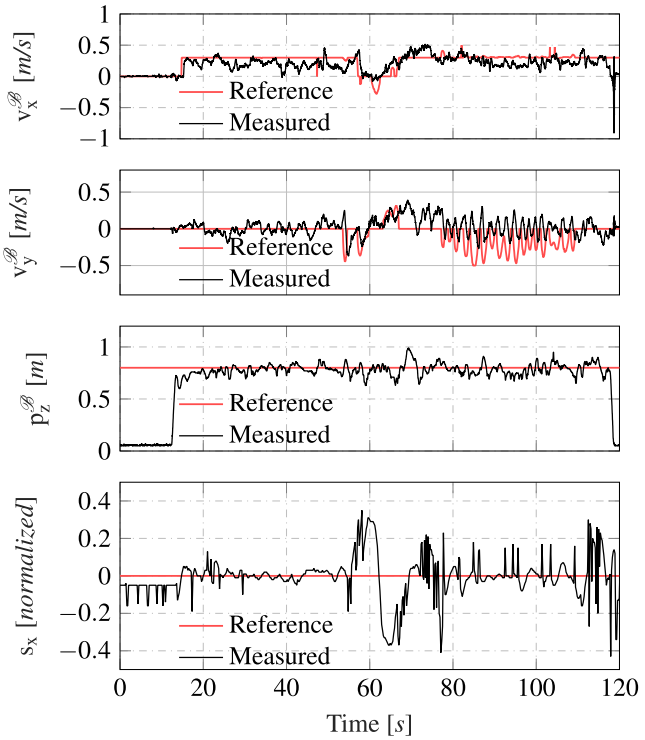

FIGURE 6. Linear velocities $v_x^{\mathcal{B}}$ and $v_y^{\mathcal{B}}$, altitude $p_z^{\mathcal{B}}$ and centroid s_x reference tracking during the navigation in the 1st scenario.

and in the majority of the experiment was close to 0.3 m/s. Nevertheless, around 60 seconds the turn was initiated and the MAV floated towards the wall, which activated the potential field reactive planner providing less or equal than 0 m/s references. The second subfigure of Figure 6 showcases the reference tracking performance of $v_y^{\mathcal{B}}$ over time. In this case the controller was able to follow the reference with Mean Absolute Error of 0.05 m/s. In this case the reactive planning from potential fields is activated more frequently, especially after the turn. The third subfigure of Figure 6, depicts the altitude of the MAV relative to the commanded reference. In this case the Mean Absolute Error was 0.05 m. The fourth and final subfigure depicts the x axis coordinate tracking of the open space. In this case the Mean Absolute Error was 0.07 units. In the majority of the flight to coordinate is close to zero, expect around the time instance 60 sec where the MAV is turning and the measurements do not have any value and are omitted. Generally, the centroid extraction has some oscillation which is negligible and does not affect the overall navigation.

The control signals (roll, pitch, and normalized thrust references) generated by the nonlinear solver are depicted at Figure 7. An interesting note in the presented responses is that that around 52 sec the timer based turn is initiated and the yawrate has been fixed to 0.2 rad/sec. Interestingly from the experiment is shown that the yawrate command after the turn takes few second to stabilize, which is affected by the depth image processing. Moreover, after the turn the velocity estimation slightly drifts leading the MAV close to the wall and causing small sign alteration on the MAV roll command.

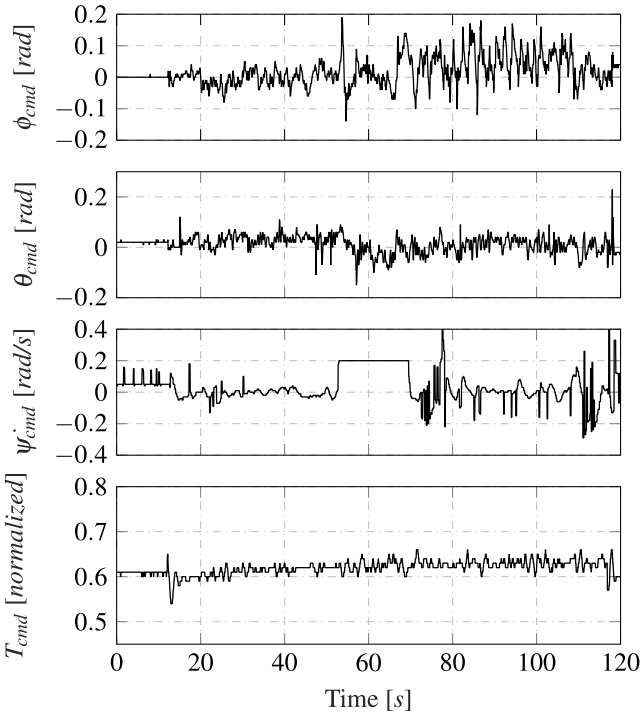

FIGURE 7. Control signals generated from the PANOC solver to the low-level controller during the navigation in the 1st scenario.

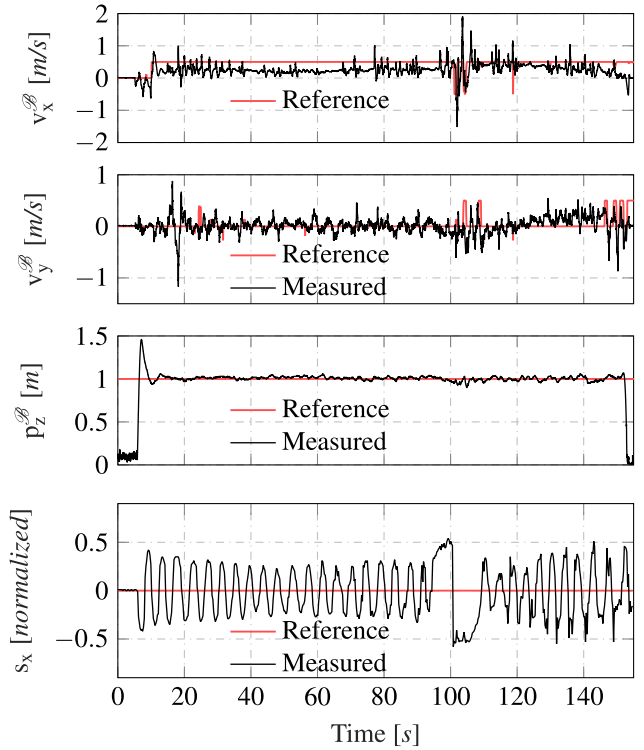

FIGURE 8. Linear velocities $v_x^{\mathcal{B}}$ and $v_y^{\mathcal{B}}$, altitude $p_z^{\mathcal{B}}$ and centroid s_x reference tracking during the navigation in the 2nd scenario.

2) SECOND SCENARIO

In this case the environment is more challenging, pitch dark, wider and with limited access. In this environment

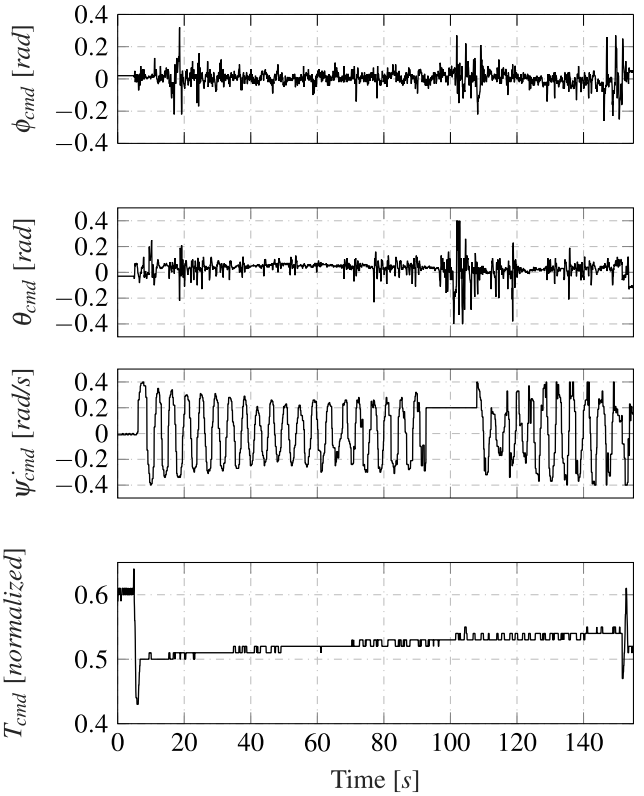

FIGURE 9. Control signals generated from the PANOC solver to the low-level controller during the navigation in the 2nd scenario.

the RealSense sensor T265 could not provide proper velocity measurements. Therefore the PX4flow sensor has been selected. The tunnel is 7 meters wide, 10 meters height and the MAV navigated for 20 meters forward and back. In this scenario the operator defined reference state vectors were $x_{ref} = [0.5\,\text{m/s}, 0, 0, 0, 0]$ and $S_{ref} = [0]$.

Similar to scenario 1, the first subfigure of Figure 8 presents the tracking of $v_x^{\mathcal{B}}$ to the desired reference. In this case the controller was able to follow the reference with Mean Absolute Error of 0.27 m/s. Although the error is higher compared to scenario 1, the MAV was still able to perform the desired task.

The second subfigure of Figure 8 showcases the reference tracking performance of v_y over time. In this case the controller was able to follow the reference with Mean Absolute Error of 0.1 m/s. Compared to scenario 1 the tunnel was wider leading to less frequent activation of the reactive potential fields, keeping v_y close to 0. Nevertheless, the potential fields were activated during the turn around the 100 sec to keep the MAV away from the tunnel surface. The third subfigure of Figure 8, depicts the altitude of the MAV relative to the commanded reference. In this case the Mean Absolute Error was 0.03 m. The forth and final subfigure depicts the x axis coordinate tracking of the open space. An important aspect to consider is that the k-means cluster selection affects the centroid extraction and an optimal clustering number is not always available. Nevertheless, although s_x was oscillating more around 0 compared to scenario 1 the MAV was able to

maintain the proper direction during the overall navigation, even after the turn. In this case the Mean Absolute Error was 0.22 units.

The control signals (roll, pitch, and normalized thrust references) generated by the nonlinear solver are depicted at Figure 9. An interesting note in the presented responses is that that around 82 sec the timer based turn is initiated and the yawrate has been fixed to 0.2 rad/sec. It is shown that the yawrate command follows the oscillatory behavior of the s_x, which is affected by the depth image processing.

In a summary, the performed experiments demonstrate the effectiveness of the vision based method to detect open spaces and align the MAV heading, facilitating the tunnel navigation. Nevertheless, the presented method is a baseline capability that can be enhanced with more features for a more robust behaviour. More specifically, the takeoff and landing can be automated using markers like apriltags, while junction detection methods can be incorporated to complement the navigation task when the tunnels have multiple branches.

IV. CONCLUSION

This article approached the problem of autonomous navigation in challenging tunnel-like environments by coupling a NMPC control architecture that aligns the robot motion along the tunnel axis. A visual processing method on both RGB-D or RGB sensors was developed to identify free space in the image plane and use it to regulate the heading of the MAV. Experimental results in a corridor as well as a harsh underground mine tunnel demonstrated the ability of the proposed system to navigate along areas that are previously unknown with the main purpose to collect raw sensor data and come back to the base. Future directions of the proposed scheme include the incorporation of breadcrumb following navigation planner (visual landmarks) on top of the control framework top allow complex navigation manoeuvres in large scale areas, while focusing in areas that either visual or lidar based odometry is not sufficiently accurate.

REFERENCES

[1] M. Eich, F. Bonnin-Pascual, E. Garcia-Fidalgo, A. Ortiz, G. Bruzzone, Y. Koveos, and F. Kirchner, "A robot application for marine vessel inspection," *J. Field Robot.*, vol. 31, no. 2, pp. 319–341, Mar. 2014.

[2] J. Qi, D. Song, H. Shang, N. Wang, C. Hua, C. Wu, X. Qi, and J. Han, "Search and rescue rotary-wing UAV and its application to the Lushan ms 7.0 earthquake," *J. Field Robot.*, vol. 33, no. 3, pp. 290–321, May 2016.

[3] S. S. Mansouri, C. Kanellakis, G. Georgoulas, D. Kominiak, T. Gustafsson, and G. Nikolakopoulos, "2D visual area coverage and path planning coupled with camera footprints," *Control Eng. Pract.*, vol. 75, pp. 1–16, Jun. 2018.

[4] A. Agha *et al.*, "NeBula: Quest for robotic autonomy in challenging environments; TEAM CoSTAR at the DARPA subterranean challenge," 2021, *arXiv:2103.11470*. [Online]. Available: https://arxiv.org/abs/2103.11470

[5] M. F. Ginting, K. Otsu, J. Edlund, J. Gao, and A.-A. Agha-Mohammadi, "CHORD: Distributed data-sharing via hybrid ROS 1 and 2 for multi-robot exploration of large-scale complex environments," *IEEE Robot. Autom. Lett.*, vol. 6, no. 3, pp. 5064–5071, Jul. 2021.

[6] K. Otsu, S. Tepsuporn, R. Thakker, T. S. Vaquero, J. A. Edlund, W. Walsh, G. Miles, T. Heywood, M. T. Wolf, and A.-A. Agha-Mohammadi, "Supervised autonomy for communication-degraded subterranean exploration by a robot team," in *Proc. IEEE Aerosp. Conf.*, Mar. 2020, pp. 1–9.

[7] K. Ebadi, Y. Chang, M. Palieri, A. Stephens, A. Hatteland, E. Heiden, A. Thakur, N. Funabiki, B. Morrell, S. Wood, L. Carlone, and A.-A. Agha-mohammadi, "LAMP: Large-scale autonomous mapping and positioning for exploration of perceptually-degraded subterranean environments," in *Proc. IEEE Int. Conf. Robot. Autom. (ICRA)*, May 2020, pp. 80–86.

[8] T. Ozaslan, G. Loianno, J. Keller, C. J. Taylor, V. Kumar, J. M. Wozencraft, and T. Hood, "Autonomous navigation and mapping for inspection of penstocks and tunnels with MAVs," *IEEE Robot. Autom. Lett.*, vol. 2, no. 3, pp. 1740–1747, Jul. 2017.

[9] C. H. Tan, D. S. B. Shaiful, W. J. Ang, S. K. H. Win, and S. Foong, "Design optimization of sparse sensing array for extended aerial robot navigation in deep hazardous tunnels," *IEEE Robot. Autom. Lett.*, vol. 4, no. 2, pp. 862–869, Apr. 2019.

[10] F. Mascarich, S. Khattak, C. Papachristos, and K. Alexis, "A multi-modal mapping unit for autonomous exploration and mapping of underground tunnels," in *Proc. IEEE Aerosp. Conf.*, Mar. 2018, pp. 1–7.

[11] D. Falanga, P. Foehn, P. Lu, and D. Scaramuzza, "PAMPC: Perception-aware model predictive control for quadrotors," in *Proc. IEEE/RSJ Int. Conf. Intell. Robots Syst. (IROS)*, Oct. 2018, pp. 1–8.

[12] A. Mcfadyen, L. Mejias, P. Corke, and C. Pradalier, "Aircraft collision avoidance using spherical visual predictive control and single point features," in *Proc. IEEE/RSJ Int. Conf. Intell. Robots Syst.*, Nov. 2013, pp. 50–56.

[13] C. Potena, D. Nardi, and A. Pretto, "Effective target aware visual navigation for UAVs," in *Proc. Eur. Conf. Mobile Robots (ECMR)*, Sep. 2017, pp. 1–7.

[14] M. Sheckells, G. Garimella, and M. Kobilarov, "Optimal visual servoing for differentially flat underactuated systems," in *Proc. IEEE/RSJ Int. Conf. Intell. Robots Syst. (IROS)*, Oct. 2016, pp. 5541–5548.

[15] P. Roque, E. Bin, P. Miraldo, and D. V. Dimarogonas, "Fast model predictive image-based visual servoing for quadrotors," in *Proc. IEEE/RSJ Int. Conf. Intell. Robots Syst. (IROS)*, Oct. 2020, pp. 7566–7572.

[16] M. Kamel, T. Stastny, K. Alexis, and R. Siegwart, "Model predictive control for trajectory tracking of unmanned aerial vehicles using robot operating system," in *Robot Operating System (ROS)*. Cham, Switzerland: Springer, 2017, pp. 3–39.

[17] E. Small, P. Sopasakis, E. Fresk, P. Patrinos, and G. Nikolakopoulos, "Aerial navigation in obstructed environments with embedded nonlinear model predictive control," in *Proc. 18th Eur. Control Conf. (ECC)*, Jun. 2019, pp. 3556–3563.

[18] F. Chaumette and S. Hutchinson, "Visual servo control. I. Basic approaches," *IEEE Robot. Autom. Mag.*, vol. 13, no. 4, pp. 82–90, Dec. 2006.

[19] C. Kanellakis, P. Karvelis, and G. Nikolakopoulos, "Open space attraction based navigation in dark tunnels for MAVs," in *Proc. 12th Int. Conf. Comput. Vis. Syst. (ICVS)*, 2019, pp. 110–119.

[20] F. Cozman and E. Krotkov, "Depth from scattering," in *Proc. IEEE Comput. Soc. Conf. Comput. Vis. Pattern Recognit.*, Jun. 1997, pp. 801–806.

[21] R. T. Tan, "Visibility in bad weather from a single image," in *Proc. IEEE Conf. Comput. Vis. Pattern Recognit.*, Jun. 2008, pp. 1–8.

[22] K. He, J. Sun, and X. Tang, "Single image haze removal using dark channel prior," *IEEE Trans. Pattern Anal. Mach. Intell.*, vol. 33, no. 12, pp. 2341–2353, Dec. 2011, doi: 10.1109/TPAMI.2010.168.

[23] P. Soille, *Morphological Image Analysis: Principles and Applications*, 2nd ed. Berlin, Germany: Springer-Verlag, 2003.

[24] S. Theodoridis and K. Koutroumbas, *Pattern Recognition*, 4th ed. Orlando, FL, USA: Academic Press, 2008.

[25] R. C. Gonzalez and R. E. Woods, *Digital Image Processing*, 3rd ed. Upper Saddle River, NJ, USA: Prentice-Hall, 2006.

[26] C. Kanellakis, S. S. Mansouri, G. Georgoulas, and G. Nikolakopoulos, "Towards autonomous surveying of underground mine using mavs," in *Proc. Int. Conf. Robot. Alpe-Adria Danube Region*. Cham, Switzerland: Springer, 2018, pp. 173–180.

[27] L. Stella, A. Themelis, P. Sopasakis, and P. Patrinos, "A simple and efficient algorithm for nonlinear model predictive control," in *Proc. IEEE 56th Annu. Conf. Decis. Control (CDC)*, Dec. 2017, pp. 1939–1944.

CHRISTOFOROS KANELLAKIS received the Ph.D. degree from the Control Engineering Group, Luleå University of Technology (LTU), Sweden, and the Diploma degree from the Department of Electrical and Computer Engineering, University of Patras (UPAT), Greece, in 2015. He is currently a Postdoctoral Researcher with the Department of Computer Science, Electrical and Space Engineering, LTU. He also works in the field of robotics, focusing on the combination of control and vision to enable robots perceive and interact with the environment.

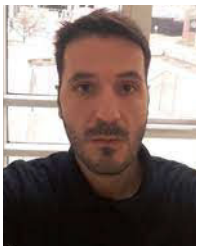

PETROS S. KARVELIS was born in Mesologi, Greece, in 1978. He received the Diploma degree and the M.Sc. and Ph.D. degrees in computer science from the University of Ioannina, Greece, in 2001, 2004, and 2012, respectively. His research interests include medical image processing, machine learning, and computer vision.

SINA SHARIF MANSOURI (Member, IEEE) received the Bachelor of Science degree from the University of Tehran, Iran, in 2012, the Master of Science degree from the Technical University of Dortmund, Germany, in 2014, and the Ph.D. degree from the Control Engineering Group, Luleå University of Technology (LTU), Luleå, Sweden, in 2020. He is currently a Postdoctoral Researcher within the Control Engineering Group, Department of Computer Science, Electrical and Space Engineering, LTU. He also works in the field of robotics, focusing on control, navigation, and exploration with multiple agents.

ALI-AKBAR AGHA-MOHAMMADI received the Ph.D. degree from Texas A&M University. He was an Autonomy Research Engineer with Qualcomm Research and a Postdoctoral Researcher with the Laboratory for Information and Decision Systems, Massachusetts Institute of Technology. He is currently a Robotics Research Technologist with the NASA's Jet Propulsion Laboratory (JPL), Caltech. He manages several projects at JPL on autonomy, control, and perception for robotic systems (rovers and aerial vehicles). His research interests include robotic autonomy, mobility and perception, stochastic control systems, and filtering theory. He was selected as a NASA NIAC Fellow, in 2018.

GEORGE NIKOLAKOPOULOS was working as a Project Manager and a Principal Investigator in several R&D&I projects funded by the EU, ESA, Swedish, and the Greek National Ministry of Research. In 2013, he has established the bigger outdoors motion capture systems in Sweden, and most probably in Europe, as part of the FROST Field Robotics Laboratory, Luleå University of Technology, Luleå, Sweden. He is currently a Professor on robotics and automation with the Department of Computer Science, Electrical and Space Engineering, Luleå University of Technology. His work is focusing in the area of robotics and control applications, while he has a significantly large experience in creating and managing European and National Research Projects. He is the Coordinator of H2020-ICT AEROWORKS project in the field of aerial collaborative UAVs and H2020-SPIRE project DISIRE in the field of integrated process control. His published scientific work includes more than 150 published international journals and conferences in the fields of his interest. In 2003, he has received the Information Societies Technologies (IST) Prize Award for the Best Paper that promotes the scopes of the European IST (currently known as ICT) sector. In 2014, he has received the 2014 Premium Award for Best Paper in *IET Control Theory and Applications*, (Elsevier) for the research work in the area of UAVs. In 2014, he has been nominated as a LTU's Wallenberg candidate, one out of three nominations from the University and 16 in total engineering nominations in Sweden. His publications in the field of UAVs have received top recognition from the related scientific community, while have been several times listed in the TOP 25 most popular publications in *Control Engineering Practice* (Elsevier).